



A spectral viscosity method for correcting the long-term behavior of POD models

S. Sirisup, G.E. Karniadakis *

Division of Applied Mathematics, Center for Fluid Mechanics, Brown University, 182 George Street, Box F, Providence, RI 01912, USA

Received 16 September 2002; received in revised form 14 August 2003; accepted 26 August 2003

Abstract

Low-dimensional flow dynamical systems may converge to erroneous states after long-time integration, even if they are initialized with the correct state. In this paper, we investigate the accuracy of such two-dimensional models constructed from Karhunen–Loeve expansions for flows past a circular cylinder. We first demonstrate that although the short-term dynamics may be predicted accurately with only a handful of modes retained, drifting of the solution may arise after a few hundred vortex shedding cycles. We then propose a dissipative model based on a spectral viscosity (SV) diffusion convolution operator. The parameters of the SV model are selected rigorously based on bifurcation analysis. Our results show that this is an effective way of improving the accuracy of long-term predictions of low-dimensional Galerkin systems.

© 2003 Elsevier B.V. All rights reserved.

1. Introduction

Proper orthogonal decomposition (POD) is a methodology that first identifies the few most energetic modes in a time-dependent system, and second provides a means of obtaining a low-dimensional description of the system's dynamics [1]. A particular effective approach is the *method of snapshots*, first proposed in [2] for flow systems, that makes the method easy to implement in practice. POD has been successfully implemented in conjunction with experimental (e.g., [3–7]) as well as with numerical studies (e.g., [2,8–13]) in thermal convection, shear layers, cavity flows and external flows, to mention just a few.

In some of the aforementioned studies ad hoc viscosity models have been incorporated to produce accurate simulations (e.g., [12] for cavity flows) while in others there was no explicit closure incorporated (e.g., [8] for cylinder flows). In particular, as the number of modes increases above a certain threshold, the POD-based model seems to be accurate at least for short-time integration. This assumes that the correct initial conditions have been used, e.g., they are derived from corresponding direct numerical simulations.

* Corresponding author. Fax: +1-401-863-3369.

E-mail address: gk@cfm.brown.edu (G.E. Karniadakis).

However, even in this case the POD model may diverge and will approach, after a long-time integration, another erroneous state. This switching of states is not an actual instability, in a sense of a catastrophic change, but rather a gradual drifting from one state to another. In this paper, we will refer occasionally to such drifting as an instability.

From the theoretical standpoint, it is well known that the system of ordinary differential equations derived from the Galerkin projection of a dissipative PDE may be unstable for the long-term dynamics, see [14]. A potential approach to restore dissipation back to the low-dimensional system is *non-linear Galerkin* projection, which is based on concepts of approximate inertial manifolds, see ([15–17]). For fully discrete systems, the non-linear Galerkin method has been shown to be stable for the long-term dynamics but some sensitivity to initial data was also revealed, see [18]. In practice, this method works effectively as it was shown recently in [19] using a low-dimensional system constructed from experimental (Particle Image Velocimetry) data. However, we have encountered several other reduced flow model systems for which such stabilization proved inadequate.

In this paper, we present an alternative closure strategy based on the spectral vanishing viscosity (SVV) method. The work was first introduced in [20] in the context of constructing *monotonicity preserving* discretizations for hyperbolic conservation laws. More recently, it has been employed successfully in formulating alternative large-eddy simulation (LES) approaches [21]. Also, in [22], the Legendre spectral vanishing method was shown to effectively control the Gibb’s phenomenon, while in [23] the SVV approach was employed in simulating two-dimensional waves in stratified atmosphere.

The spectral vanishing viscosity approach guarantees an essentially non-oscillatory behavior although some small oscillations of *bounded amplitude* may be present in the solution. This theory is based on three key components:

1. A vanishing viscosity amplitude which decreases with the mode number.
2. A viscosity-free spectrum for the lower, most energetic modes.
3. An appropriate viscosity kernel for the high-wave numbers.

SVV is especially suitable for *hierarchical discretizations*, such as ones obtained via the proper orthogonal decomposition, where global energetically-ordered modes are involved. This implies that SVV preserves the inherent energetic scale separation while it also maintains monotonicity of the total variation bounded (TVB) kind by controlling the high-frequency components. This effective regularization is determined by parameters whose range is guided by the theory for advection-dominated systems. More recent work has extended the method to superviscosity formulations, first by Tadmor [24] and later by Ma [25,26], in order to extend the range of the *viscosity-free* spectrum.

In the following, we first demonstrate a few cases where instabilities (i.e., solution drifts) arise. Subsequently, we introduce the SVV method and modify its amplitude in order to make the method effective for POD systems. In particular, we develop a new procedure in selecting *rigorously* the free parameters that guarantee accurate asymptotic states of the low-dimensional system.

2. Mathematical formulation

2.1. Direct numerical simulation

We consider here flow past a circular cylinder for which both two- and three-dimensional POD models have been constructed in [8] and [27], respectively. With initial conditions obtained from corresponding direct numerical simulations, these models were shown to be accurate for tens and even hundreds of shedding cycles without incorporating any closure model. Here, we will re-examine the accuracy of the POD predictions for these flows. In particular, for the concepts developed here, we consider *two-dimensional* uniform flow past a circular cylinder at Reynolds number $Re = 100$ and $Re = 500$.

The computational domain is shown in Fig. 1. Uniform steady or time-dependent boundary conditions are imposed at the inflow boundary Γ_1 . Uniform velocity is also imposed on Γ_3 and Γ_4 while on Γ_2 the zero Neumann condition on velocity is imposed. On the cylinder surface Γ_5 the no-slip boundary condition is prescribed. Converged solutions were obtained using the spectral/*hp* element method [28]. Typical results that show the differences in spatial scales in terms of vorticity at $Re = 100$ and $Re = 500$ are shown in Fig. 2.

2.2. POD models

We employed 50 snapshots of DNS data in order to construct low-dimensional models using the proper orthogonal decomposition. We briefly review this procedure next.

Let us decompose the total flow field \mathbf{V} as

$$\mathbf{V}(\mathbf{x}, t) = \mathbf{U}_0(\mathbf{x}) + \mathbf{u}(\mathbf{x}, t),$$

where \mathbf{U}_0 is the *time-averaged* field.

Then, we extract the POD modes, based on the DNS data, which are eigenvectors of a covariance matrix \mathbf{C} ; its elements are computed as follows

$$c_{i,j} = \int \mathbf{u}(\mathbf{x}, t_i) \cdot \mathbf{u}(\mathbf{x}, t_j) d\mathbf{x} = \int \int (u(x, y, t_i)u(x, y, t_j) + v(x, y, t_i)v(x, y, t_j)) dx dy,$$

where u, v are the two components of the velocity vector \mathbf{u} . This is the *snapshot method formulation*. The matrix \mathbf{C} represents the correlation between temporal points since the spatial variable has been integrated out. We then compute the eigenvectors of the above covariance matrix, denoted by \mathbf{a} , and the POD modes denoted by $\phi(x, y)$. Specifically, the vector $\phi(x, y)$ is given by

$$\phi_u(x, y)_j = \sum_{i=1}^N a_j(t_i)u(x, y, t_i),$$

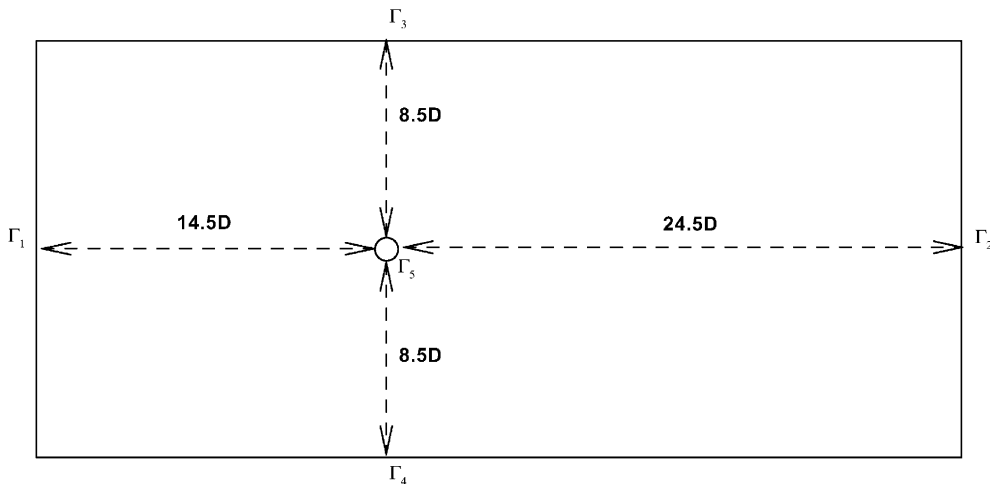


Fig. 1. Computational domain.

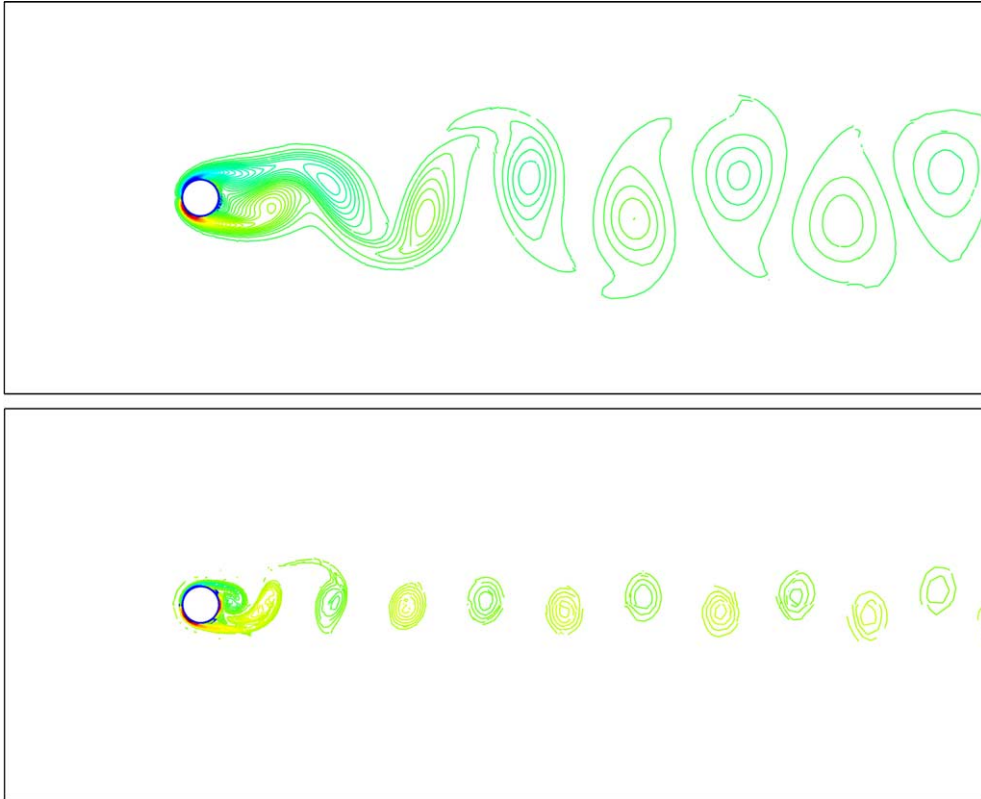


Fig. 2. Instantaneous vorticity contours at $Re = 100$ (upper) and $Re = 500$ (lower).

$$\phi_v(x, y)_j = \sum_{i=1}^N a_j(t_i) v(x, y, t_i),$$

where N is the total number of snapshots, ϕ_u and ϕ_v are the components of the vector $\phi(x, y)$, and j is the mode index. The corresponding energy distribution of POD modes is plotted in Fig. 3 for $Re = 100$ and $Re = 500$.

We employ the hierarchical POD modes obtained from the DNS data as a basis to represent the velocity field. In addition, we employ a Galerkin projection of the Navier–Stokes equations onto spatial modes to obtain the system of ordinary differential equation that governs the dynamics of the system.

We express the two-dimensional field \mathbf{u} as the linear combination of the POD modes

$$u(x, y, t) = \sum_{j=1}^N \phi_u(x, y)_j a_j(t),$$

$$v(x, y, t) = \sum_{j=1}^N \phi_v(x, y)_j a_j(t),$$

where $a_j(t)$ are the unknown coefficients. The Galerkin projection of the Navier–Stokes equations gives

$$\int \phi \cdot \left(\frac{\partial \mathbf{V}}{\partial t} + (\mathbf{V} \cdot \nabla) \mathbf{V} + \nabla p - \frac{1}{Re} \nabla^2 \mathbf{V} \right) dx = 0, \quad (1)$$

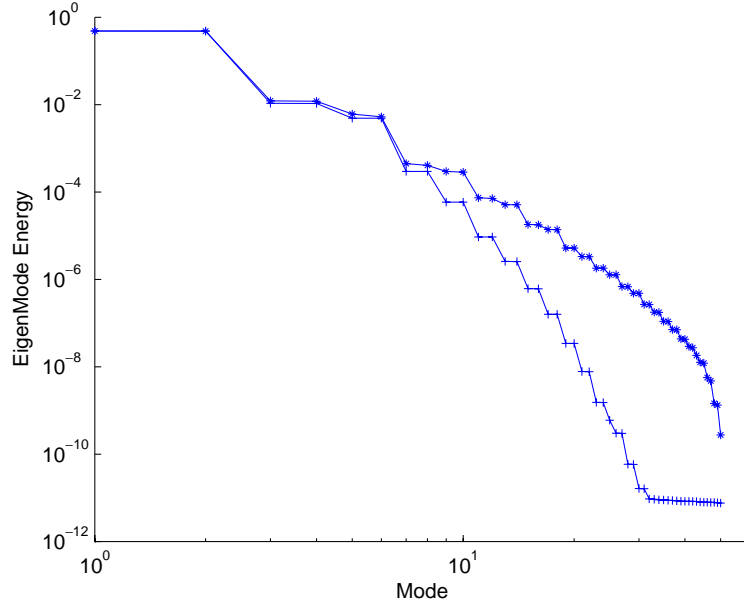


Fig. 3. Energy distribution of POD modes for $Re = 100$ (+) and $Re = 500$ (*).

where the projection vector is $\boldsymbol{\phi} = [\phi_u, \phi_v]^T$, extracted from DNS. We use the divergence-free eigenmodes so the pressure term inside the domain is eliminated via integration by parts. Also the Dirichlet and the outflow conditions imposed at the boundaries lead to the vanishing of contributions from the pressure on those boundaries in the integration by parts procedure.

A Galerkin projection leads to the dynamical system:

$$\frac{\partial \mathbf{a}_j(t)}{\partial t} = f_j(\mathbf{a}) \quad (2)$$

with $\mathbf{a} = [a_1, a_2, \dots]$. The term $f_j(\mathbf{a})$ includes the convective and viscous terms and has the form:

$$f_j(\mathbf{a}) = - \left(\int \boldsymbol{\phi}_j \nabla \cdot (\boldsymbol{\phi}_i \boldsymbol{\phi}_k) \, d\mathbf{x} \right) a_i a_k - \left(\frac{1}{Re} \int \nabla \boldsymbol{\phi}_j \nabla \boldsymbol{\phi}_i \, d\mathbf{x} + \int \boldsymbol{\phi}_j \nabla \cdot (\boldsymbol{\phi}_i \mathbf{U}_0) \, d\mathbf{x} \right. \\ \left. + \int \boldsymbol{\phi}_j \nabla \cdot (\mathbf{U}_0 \boldsymbol{\phi}_i) \, d\mathbf{x} \right) a_i - \left(\int \boldsymbol{\phi}_j \nabla \cdot (\mathbf{U}_0 \mathbf{U}_0) \, d\mathbf{x} + \frac{1}{Re} \int \nabla \boldsymbol{\phi}_j \nabla \mathbf{U}_0 \, d\mathbf{x} \right).$$

In the following we investigate the time evolution of the modal coefficients $a_j(t), j = 1, 2, \dots, N$.

3. Accuracy of POD flow models

First, we present results from the long-time integration of the $Re = 100$ case with steady uniform inflow. The magnitudes of first two most energetic modes from the DNS are presented in Table 1. It was found in [8] that a 6-mode POD system (initialized with DNS data) gives accurate results in comparison with DNS data, at least for the short-time dynamics. Indeed, various reduced models we tested again with $N \geq 6$ are accurate after short-time integration. This is demonstrated in Table 2, where the magnitudes of the first two modes are presented. This accuracy is maintained for times up to several hundreds of shedding cycles. Also,

Table 1
Oscillation period and the first two most energetic modes from DNS

$Re = 100$		$Re = 500$	
Magnitudes	Period	Magnitudes	Period
$\bar{a}_1 = 2.656$	$T = 5.89$	$\bar{a}_1 = 4.192$	$T = 4.385$
$\bar{a}_2 = 2.653$		$\bar{a}_2 = 4.277$	

Table 2
Magnitudes of the first two most energetic modes from POD simulations for $Re = 100$

N	Energy captured (%)	Short-term dynamics		Long-term dynamics	
		\bar{a}_1	\bar{a}_2	\bar{a}_1	\bar{a}_2
6	99.9269	2.6524	2.6532	2.158	2.155
10	99.9975	2.6558	2.6533	16.523	16.667
20	100	2.6560	2.6534	16.506	16.615

by comparing the values in Tables 1 and 2 we see that the more POD modes included in the POD model the more accurate is the prediction of the short-term dynamics.

Our experiments, however, show that all models converge asymptotically to a different attractor. This is consistent with the findings of Aubry et al. [29] for the Kuramoto–Sivashinsky equation (KSE). They observed that even with a POD model that captures more than 99.99% of energy the predicted solution does not converge to the right attractor. In flow past a cylinder, a 6-mode system (initialized with the DNS data) is accurate for up to 40 shedding cycles (about 200 convective time units) as shown in Fig. 4 but it diverges to a different attractor for time $t > 200$. As the number of modes increases the accuracy of the model is enhanced. Thus, a 10-mode system is accurate for up to 500 shedding cycles, i.e., more than 3000

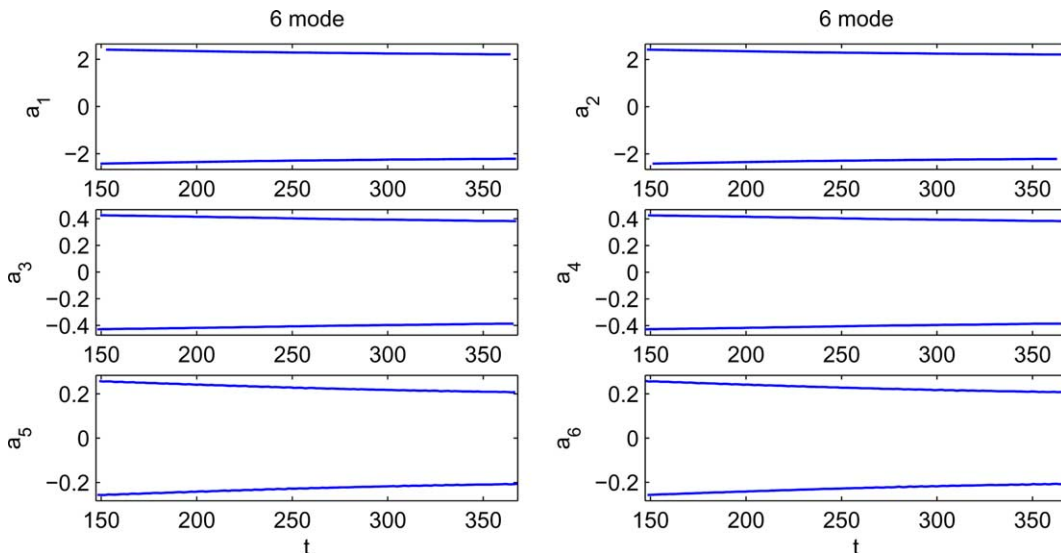


Fig. 4. $Re = 100$. Envelopes of the time history showing the onset of divergence in the 6-mode POD system. The oscillation corresponds to period $T = 5.88$.

convective time units, but eventually all modes show drifting as shown in Fig. 5. However, for the first 50 shedding cycles the POD predictions are in very good agreement with the DNS data as shown in Fig. 6. This long-term inaccurate prediction occurs even though the POD models capture almost 100% of the energy for large N (see Table 2). In contrast, the results for KSE by [29] show that with the addition of one extra mode the correct asymptotic dynamics is predicted.

The exact onset of divergence from the correct limit cycle depends on the number N of modes retained in the reduced model. For the results presented in Table 2, we have integrated up to 1000 shedding cycles both models with $N = 6$ and $N = 10$ achieving asymptotic states. However, the model with $N = 20$ is still in the transient state with $\bar{a}_1 = 2.8150$ and $\bar{a}_2 = 2.8124$ after 1000 shedding cycles. The asymptotic values of the magnitudes of the $N = 20$ model are shown in Table 2(right); they were obtained after integration for at least 3000 shedding cycles.

The divergence from the correct limit cycle of the POD model also depends on the Reynolds number. At the higher Reynolds number ($Re = 500$) the onset of divergence arises earlier even for a higher-order model. For example, in Fig. 7 we show the time history of the modes for a 20-mode POD model. The divergence here sets in at about 100 shedding cycles into the time integration. This result is typical of several other models we constructed for the uniform steady inflow.

However, not all low-dimensional systems have erroneous long-term behavior. Our experiments show that *non-autonomous systems*, i.e., systems with an imposed time scale through external forcing, may be

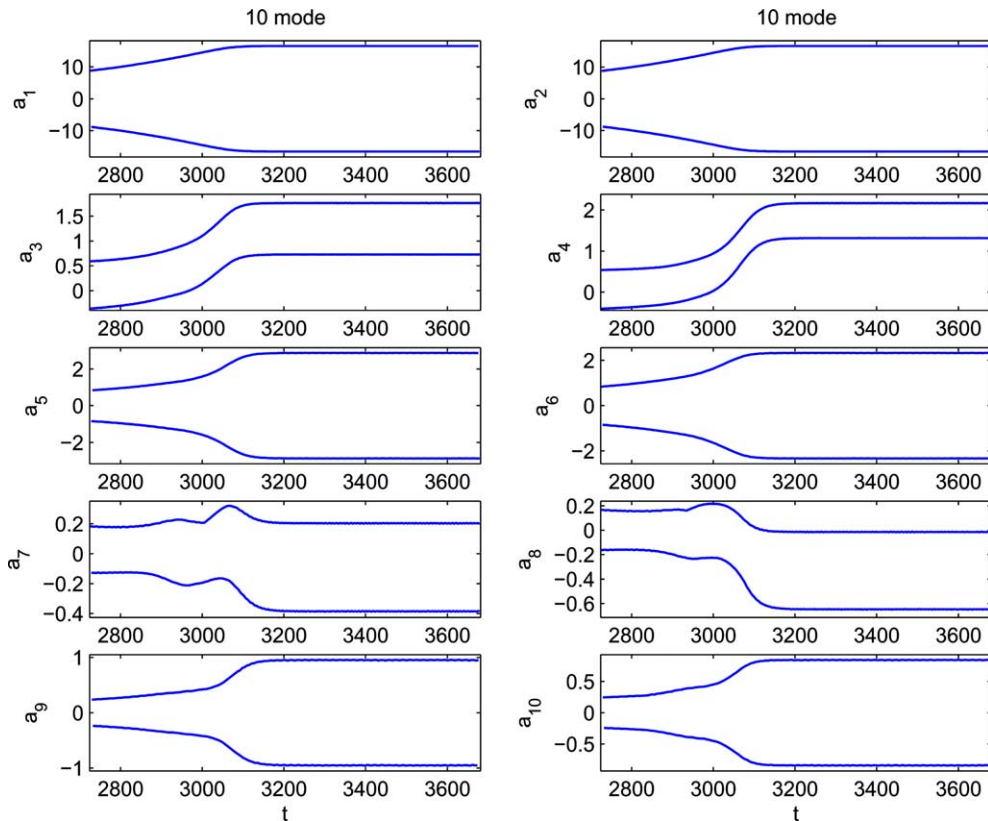


Fig. 5. $Re = 100$. Envelopes of the time history showing the onset of divergence in the 10-mode POD system. The oscillation corresponds to period $T = 5.84$.

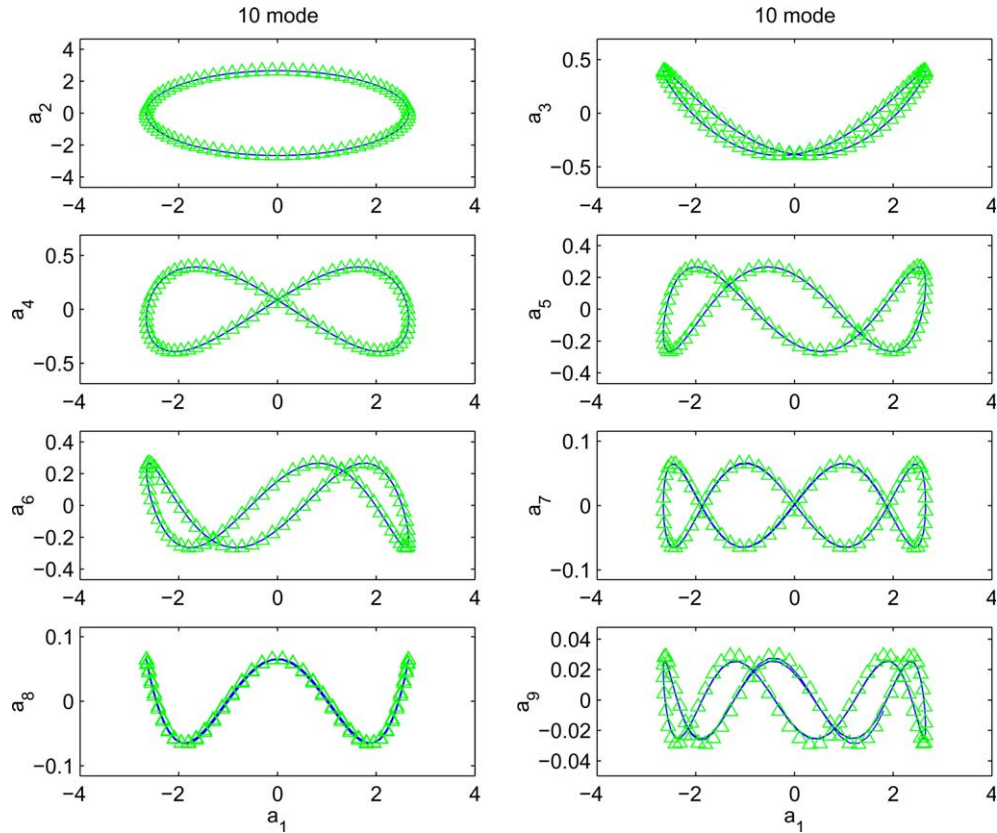


Fig. 6. $Re = 100$. Phase portrait during the first 50 shedding cycles for the 10-mode system. The lines denote POD predictions and the triangles correspond to DNS data.

asymptotically accurate at *all* times. To this end, we consider the flow past a cylinder again at $Re = 500$ but with a small sinusoidal velocity component added at the inflow, with 10% amplitude forced at the Strouhal frequency. The resulting POD system predicts the expected lock-in state, in agreement with DNS, and it is asymptotically accurate even for $N = 12$, see Fig. 8 and also [30] for more details. The time history shows that the accuracy of the POD prediction is maintained for all times. The Galerkin model in the unsteady inflow case is based on a modification of the system of Eq. (2) to include a penalty term that facilitates the time-dependent boundary conditions in the reduced POD system.

4. The spectral vanishing viscosity model

Tadmor [20] first introduced the concept of spectral vanishing viscosity (SVV) using the inviscid Burgers' equation. The distinct feature of solutions to this problem is that spontaneous jump discontinuities (shock waves) may be developed, and hence a *class* of weak solutions can be admitted. Within this class, there are many possible solutions, and in order to single out the physically relevant one an additional entropy condition is applied.

In low-dimensional systems it has been found that unstable behavior is associated with multiple spurious steady states [14], and this is consistent with the above observation. Tadmor [20] introduced the spectral

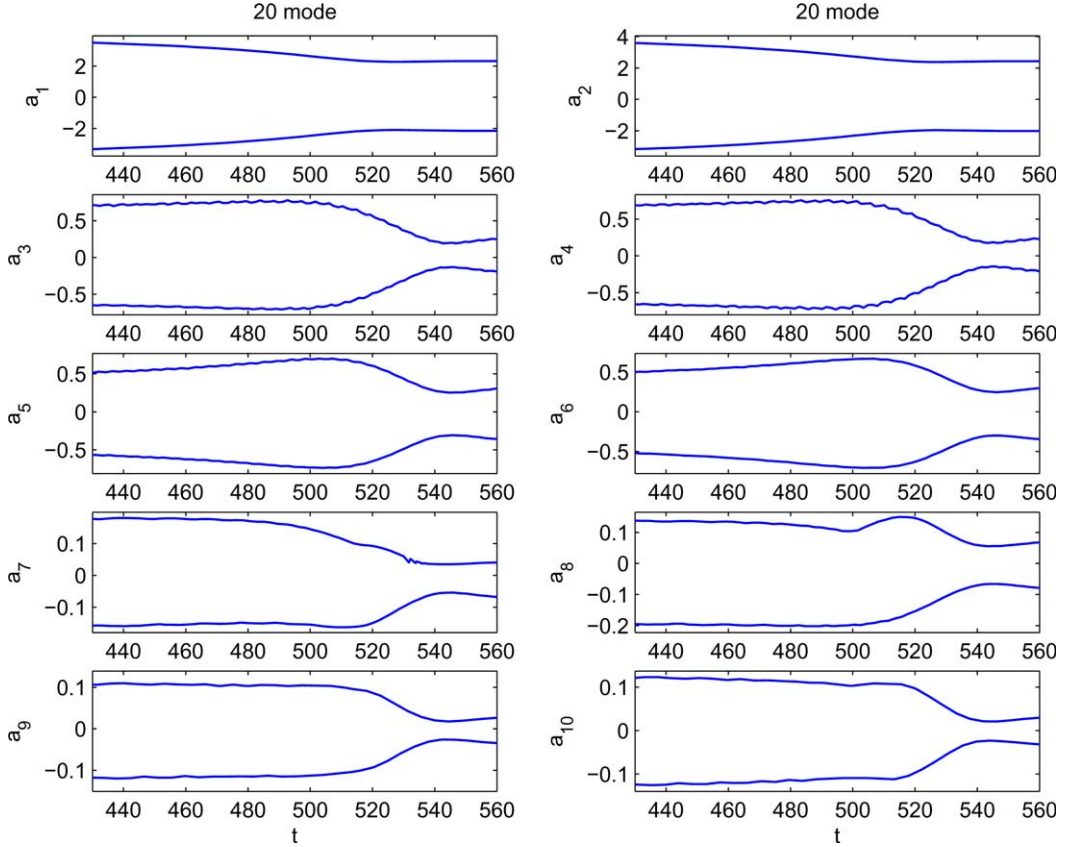


Fig. 7. $Re = 500$; *steady inflow*. Envelopes of the time history showing the onset of divergence in the 20-mode POD model. The oscillation corresponds to period $T = 4.332$.

vanishing viscosity method, which adds a small amount of *mode-dependent* dissipation that satisfies the entropy condition, yet retains spectral accuracy. It is based on viscosity solutions of non-linear Hamilton–Jacobi equations, which have been studied systematically in [31]. Specifically, the viscosity solution for the Burgers’ equation has the form

$$\frac{\partial}{\partial t} u(x, t) + \frac{\partial}{\partial x} \left(\frac{u^2(x, t)}{2} \right) = \epsilon \frac{\partial}{\partial x} \left[Q_\epsilon \frac{\partial u}{\partial x} \right], \quad (3)$$

where $\epsilon (\rightarrow 0)$ is a viscosity amplitude and Q_ϵ is a viscosity kernel. Convergence may then be established by compactness estimates combined with entropy dissipation arguments [20]. To respect spectral accuracy, the SVV method makes use of viscous regularization, and Eq. (3) may be rewritten in discrete form (retaining N modes) as in our POD model

$$\frac{\partial}{\partial t} u_N(x, t) + \frac{\partial}{\partial x} \left[\mathcal{P}_N \left(\frac{u^2(x, t)}{2} \right) \right] = \epsilon \frac{\partial}{\partial x} \left[Q_N * \frac{\partial u_N}{\partial x} \right], \quad (4)$$

where the star (*) denotes convolution and \mathcal{P}_N is a projection operator. Q_N is a viscosity kernel, which is only activated for high-wave numbers. In Fourier space, this kind of spectral viscosity can be efficiently implemented as multiplication of the Fourier coefficients of u_N with the Fourier coefficients of the kernel Q_N , i.e.,

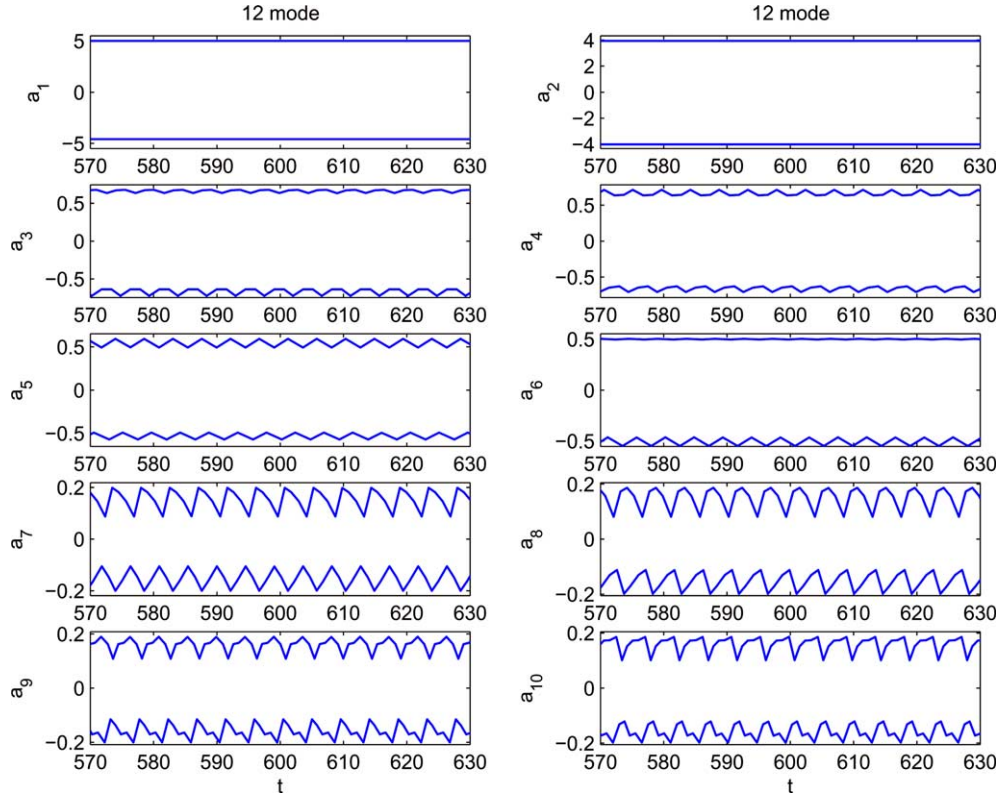


Fig. 8. $Re = 500$; oscillatory inflow. Envelopes of the time history showing asymptotic stability for the 12-mode POD model. The oscillation corresponds to period $T = 4.545$.

$$\epsilon \frac{\partial}{\partial x} \left[\mathcal{Q}_N * \frac{\partial u_N}{\partial x} \right] = -\epsilon \sum_{M \leq |k| \leq N} k^2 \hat{Q}_k(t) \hat{u}_k(t) e^{ikx},$$

where k is the wave number, N the number of Fourier modes, and M the wavenumber above which the spectral vanishing viscosity is activated. In the POD context, we also assume that this implementation of convolution is valid in the modal space.

Originally, Tadmor [20] used

$$\hat{Q}_k = \begin{cases} 0, & |k| \leq M, \\ 1, & |k| > M, \end{cases} \quad (5)$$

with $\epsilon M \sim 0.25$ based on the consideration of minimizing the total-variation of the numerical solution. In subsequent work, however, a smooth kernel was used, since it was found that the C^∞ smoothness of \hat{Q}_k improves the resolution of the SVV method. For Legendre pseudo-spectral methods, Maday et al. [32] used $\epsilon \approx N^{-1}$, activated for modes $k > M \approx 5\sqrt{N}$, with

$$\hat{Q}_k = e^{-(k-N)^2/(k-M)^2}, \quad k > M. \quad (6)$$

In order to see the difference between the convolution operator on the right-hand-side in Eq. (4) and the usual viscosity regularization, following Tadmor [33], we expand as

$$\epsilon \frac{\partial}{\partial x} \left[Q_N * \frac{\partial u_N}{\partial x} \right] = \epsilon \frac{\partial^2 u_N}{\partial x^2} - \epsilon \frac{\partial}{\partial x} \left[R_N(x, t) * \frac{\partial u_N}{\partial x} \right], \quad (7)$$

where

$$R_N(x, t) \equiv \sum_{k=-N}^N \hat{R}_k(t) e^{ikx}; \quad \hat{R}_k(t) \equiv \begin{cases} 1 - \hat{Q}_k(t), & |k| \geq M, \\ 1, & |k| < M. \end{cases} \quad (8)$$

The extra term appearing in addition to the first standard viscosity term makes this method different. It measures the distance between the spectral viscosity and the standard viscosity. This term is bounded in the L_2 norm similarly to the spectral projection error. Tadmor refers to the viscosity as vanishing as his theory requires that

$$\epsilon \approx \frac{1}{N^\theta \log N}, \quad \theta \leq 1$$

and thus $\epsilon \rightarrow 0$ for the high-resolution limit. However, in severely truncated expansions this may not be true, so in the current work we will leave ϵ a free parameter to be determined.

The implementation of the SVV in the POD models (Eq. (2)) is similar to the implementation of Fourier methods presented above or the spectral/ hp element discretization in [21]. In particular, the system of ordinary differential equations is enhanced as follows

$$\frac{\partial \mathbf{a}_j}{\partial t} = f_j(\mathbf{a}) - h_j(\mathbf{a}), \quad (9)$$

where $f_j(\mathbf{a})$ has the form presented in Eq. (3), and $h_j(\mathbf{a})$ contains the viscosity convolution kernel, i.e.,

$$h_j(\mathbf{a}) = \epsilon \hat{Q}_j \left[\int \frac{\partial \mathbf{U}_0}{\partial \mathbf{x}} \frac{\partial \phi_j}{\partial \mathbf{x}} d\mathbf{x} + \sum_{i=1}^N a_i(t) \int \frac{\partial \phi_i}{\partial \mathbf{x}} \frac{\partial \phi_j}{\partial \mathbf{x}} d\mathbf{x} \right]. \quad (10)$$

In this derivation, integration by parts is used and the fact that boundary contributions vanish because of the specific boundary conditions employed. In view of Eq. (10), we can see that only the higher modes, i.e., mode numbers greater than M , will be affected by the viscosity kernel.

We also introduce a small modification to the SVV model by setting $\epsilon = \alpha/N$ and including a free parameter a in Eq. (8), as follows:

$$\frac{\alpha}{N} \frac{\partial}{\partial x} \left[Q_N * \frac{\partial u_N}{\partial x} \right] = \frac{\alpha}{N} \frac{\partial^2 u_N}{\partial x^2} - \frac{\alpha}{N} \frac{\partial}{\partial x} \left[R_N(x, t) * \frac{\partial u_N}{\partial x} \right], \quad (11)$$

where

$$R_N(x, t) \equiv \sum_{k=-N}^N \hat{R}_k(t) e^{ikx}; \quad \hat{R}_k(t) \equiv \begin{cases} a - \hat{Q}_k(t), & |k| \geq M, \\ a, & |k| < M. \end{cases} \quad (12)$$

We will refer to the above model as “parameterized spectral viscosity” model (or parameterized SV) since we will allow for diffusion kernels with non-vanishing viscosity amplitude. We also introduce the term “standard spectral viscosity” model (or standard SV). This also corresponds to non-vanishing viscosity, and thus it is different from the SVV model given in Eqs. (7) and (8).

5. Accuracy of SV-POD flow models

Here, we demonstrate the effect of SV by revisiting the flow examples already presented in Section 2 for cylinder flow. For the comparisons that follow we will need the amplitudes of the first two most energetic modes at $Re = 100$ and $Re = 500$. In Table 1 we present those results along with the Strouhal period T . In

the following, we first consider the case where the SV parameters are chosen empirically. Subsequently, we present a new procedure to obtain the SV parameters more rigorously using bifurcation analysis.

5.1. Empirical SV model

The parameters of the SV model were chosen guided by the general theoretical estimates and also by obtaining the *best agreement* with the original data for the first 50 shedding cycles. Specifically, we have investigated the accuracy of the low-dimensional POD systems at $Re = 100$ and $Re = 500$ at different values of the wave cut-off parameter M and the best value for ϵ according to the above criterion. The detailed results can be found in [30].

Here we only present results for the higher Reynolds number $Re = 500$ for which the 20-mode POD Galerkin system ($N = 20$) diverges at earlier times. The standard SV model can effectively maintain the accuracy in the simulation. In Fig. 9 we plot the phase portrait of the first nine modes for the *first 1000 shedding cycles* in the simulation. We see that a limit cycle is predicted in excellent agreement with the DNS data. To appreciate the effect of SV in the current simulation we also present in Fig. 10 the corresponding results without SV from the pure POD Galerkin system for the same time period, which clearly diverges. In this case the cut-off mode was set to $M = 16$ and the viscosity kernel $\epsilon = \alpha/N$ was chosen to be $\epsilon = 0.0320520703$. Using a standard artificial viscosity approach, the POD Galerkin model does not lead to accurate results; in this particular case we could not obtain accurate results within the first 1000 shedding cycles.

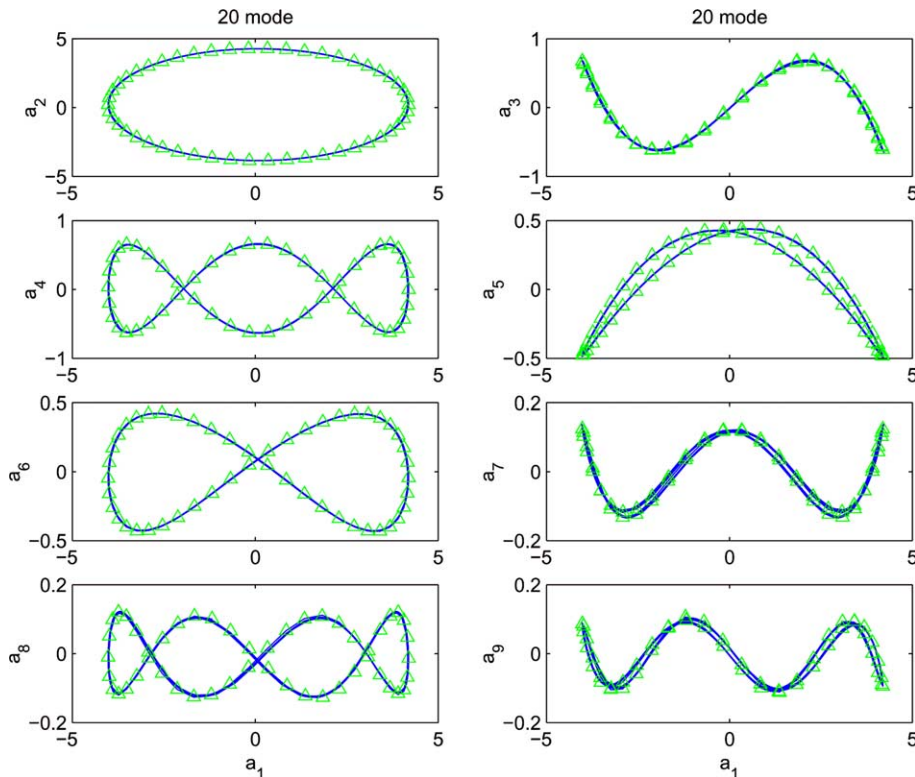


Fig. 9. $Re = 500$. Phase portrait of the first 9 modes versus the first mode in the 20-mode SV-POD system (lines) compared to the DNS data (symbols). Time integration over 1000 shedding cycles.

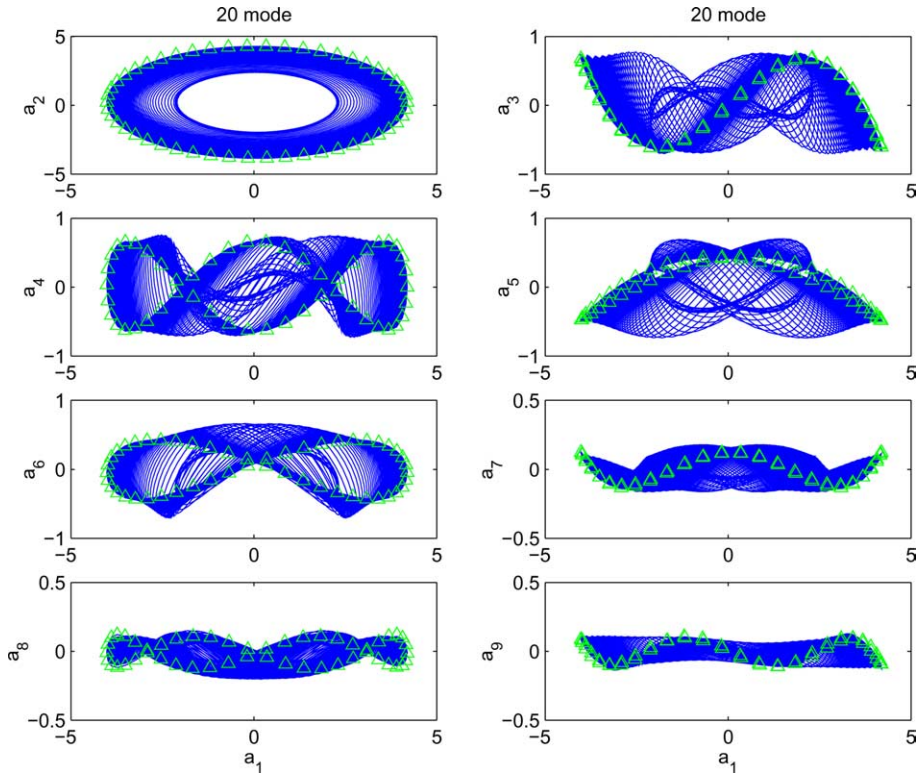


Fig. 10. $Re = 500$. Phase portrait of the first 9 modes versus the first mode in the 20-mode POD only system (lines) compared to the DNS data (symbols). Time integration over 1000 shedding cycles.

In order to also investigate the effect of SV on the higher modes we plot separately in Figs. 11 and 12 the phase portraits up to the 17th and 20th mode, respectively. We see that after the cut-off mode $M = 16$ some inaccuracies are introduced, which are more pronounced in the modes 18, 19 and 20. However, the amplitude of those modes is bounded in contrast to the high POD modes of the reduced system without any SV.

Despite the improved results of the SV-POD system constructed following the aforementioned empirical approach, its asymptotic accuracy is still questionable. Indeed, performing much longer simulations for the case we presented above we observed a divergence and eventual development of another limit cycle after integrating several thousands of shedding cycles. To address this issue we employ bifurcation analysis, based on which we can choose the appropriate values for the parameters of the SV model. This is presented in the next section.

5.2. Asymptotically accurate SV model

In order to find the proper value of the viscosity coefficient in the SV model we employ bifurcation analysis using the code AUTO, (see [34]). Specifically, we are interested in determining first if the low-dimensional system we consider exhibits a Hopf bifurcation point or if we can obtain a stable periodic solution even if it is inaccurate. Based on either of these states, we can then track the corresponding periodic branch. The key idea is to perform the bifurcation analysis with respect to α , i.e., the coefficient that determines the viscosity amplitude $\epsilon = \alpha/N$.

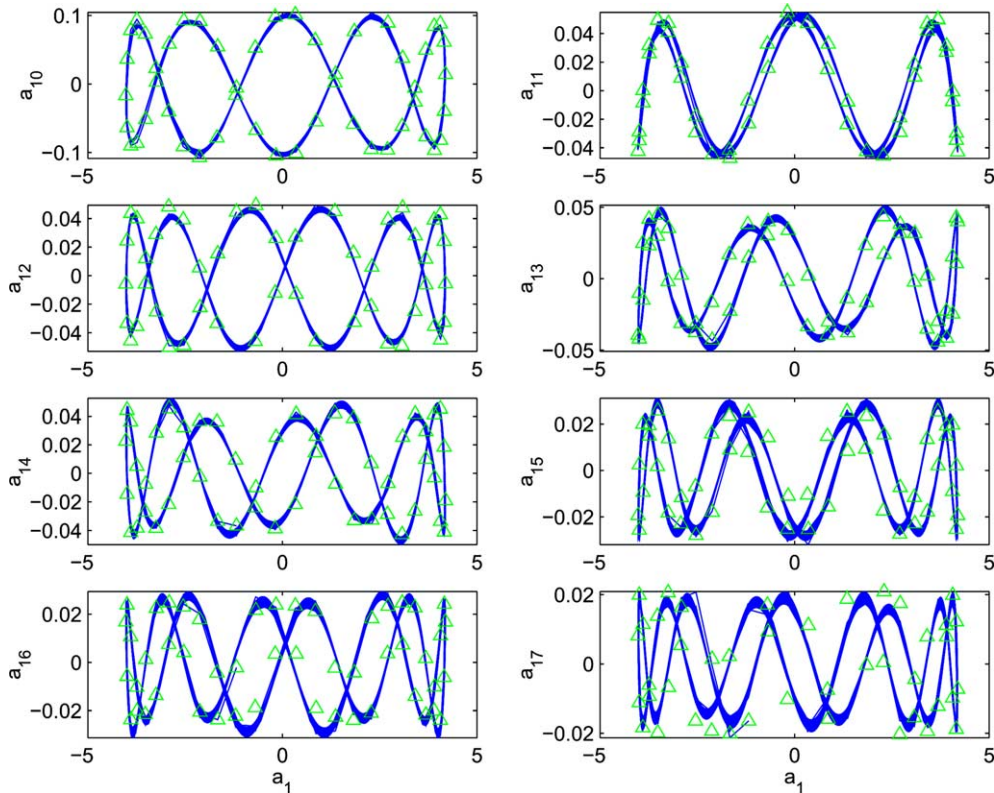


Fig. 11. $Re = 500$. Phase portrait of modes 10–17 versus the first mode in the 20-mode SV-POD system (lines) compared to the DNS data (symbols). Time integration over 1000 shedding cycles.

First, we examined the accuracy of the original 6-mode POD system corresponding to $\alpha = 0$, i.e., no SV model is incorporated. In Table 3 we summarize the results for $Re = 100$ and $Re = 500$. The magnitudes of Floquet multipliers are less than unity (except the first one which is unity), therefore the periodic solution of the original POD system is asymptotically stable. However, its asymptotic limit cycle is different than the one that DNS predicts. For $Re = 500$ the asymptotic state is characterized by a period $T = 4.33$, which is close to the DNS result ($T_{\text{DNS}} = 4.385$). However, the amplitudes of the first two modes are very different from the amplitudes of the modes corresponding to DNS, the latter having the values $\bar{a}_1 = 4.192$ and $\bar{a}_2 = 4.277$. Therefore, solving the initial value problem with no SV incorporated leads to a solution which is different than the correct limit cycle as predicted by DNS. For $Re = 100$ the situation is similar although the difference in modal amplitudes is smaller and thus it will take much longer for the POD simulation to reach the asymptotic state.

Next, we performed bifurcation analysis on the 6-mode POD system using the standard SV model at different values of the cut-off mode M . However, we could not find any Hopf bifurcation points for such systems (as we increase α to 10^7) except for the case $M = 0$. To this end, we then modified slightly the low-dimensional system by incorporating the *parameterized SV model* setting $a = 0.999$ instead of its standard value $a = 1$ in the original model [20]. For different values of the cut-off mode M of the parameterized SV model, we were able to find the Hopf bifurcation point; we then tracked the periodic branch back to the original POD system corresponding to $\alpha = 0$.

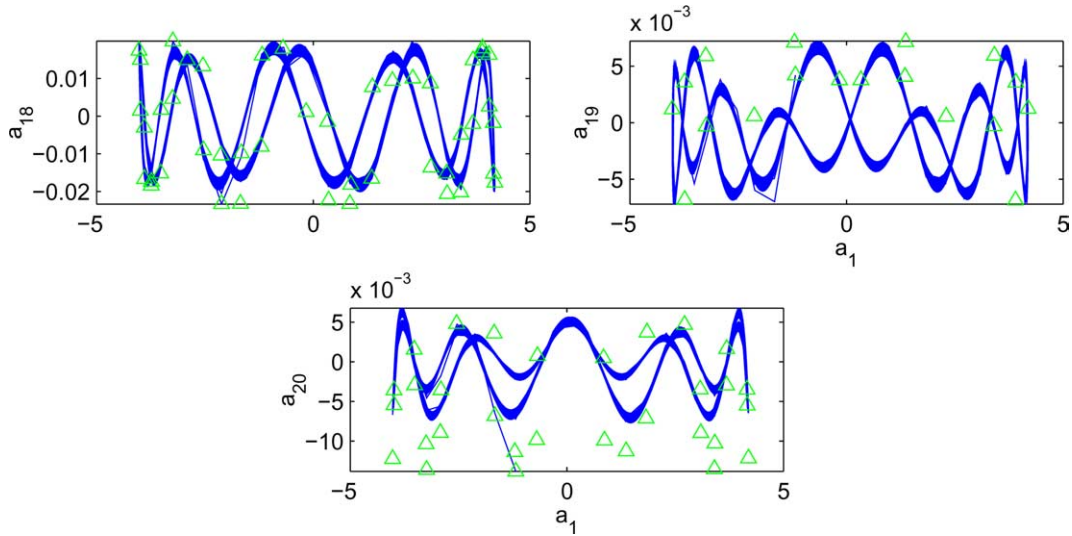


Fig. 12. $Re = 500$. Phase portrait of modes 18–20 versus the first mode in the 20-mode SV-POD system (lines) compared to the DNS data (symbols). Time integration over 1000 shedding cycles.

Table 3
Parameters for the asymptotically stable periodic solution of the original 6-mode POD system ($\alpha = 0$)

$Re = 100$			$Re = 500$		
Period	Magnitudes	Multipliers	Period	Magnitudes	Multipliers
$T = 5.88$	$\bar{a}_1 = 2.157$	$9.528E-01$	$T = 4.33$	$\bar{a}_1 = 2.380$	$9.447E-01$
	$\bar{a}_2 = 2.155$	$5.802E-01$		$\bar{a}_2 = 2.493$	$-8.035E-01 - 2.470E-01i$
		$5.635E-01$			$-8.035E-01 + 2.470E-01i$
		$-5.070E-01 - 1.690E-01i$			$7.075E-01 + 3.858E-01i$
		$-5.070E-01 + 1.690E-01i$			$7.075E-01 - 3.858E-01i$

Shown are the first two most energetic modes and the non-trivial Floquet multipliers.

Having obtained the periodic branch does not necessarily lead to a unique choice for the bifurcation parameters. Therefore, other criteria need to be invoked. Here we choose to match the amplitude \bar{a}_1 of the first mode with the DNS results, and this will lead to at most two possible solutions. Enforcing the Strouhal period to be the same in the DNS and in the bifurcation analysis yields a unique set of SV parameters. In the particular flow that we study here, the POD modes form approximate pairs and thus the second mode will match the DNS results as well. Thus, the two most energetic modes match with the DNS-based results.

First we present results for the parameterized SV model. All the calculations have been done using the maximum accuracy available for AUTO. Typical bifurcation diagrams for $Re = 100$ are shown in Fig. 13 for cut-off modes $M = 2$ (left) and $M = 4$ (right). Similar plots are shown in Fig. 14 for $Re = 500$. In particular, we can follow the aforementioned selection process of SV parameters given the DNS value for \bar{a}_1 to be 2.656 and 4.192 for $Re = 100$ and 500, respectively. In Table 4 we list the best values of the viscosity coefficient α that determines the viscosity amplitude $\epsilon = \alpha/N$ in the parameterized SV model.

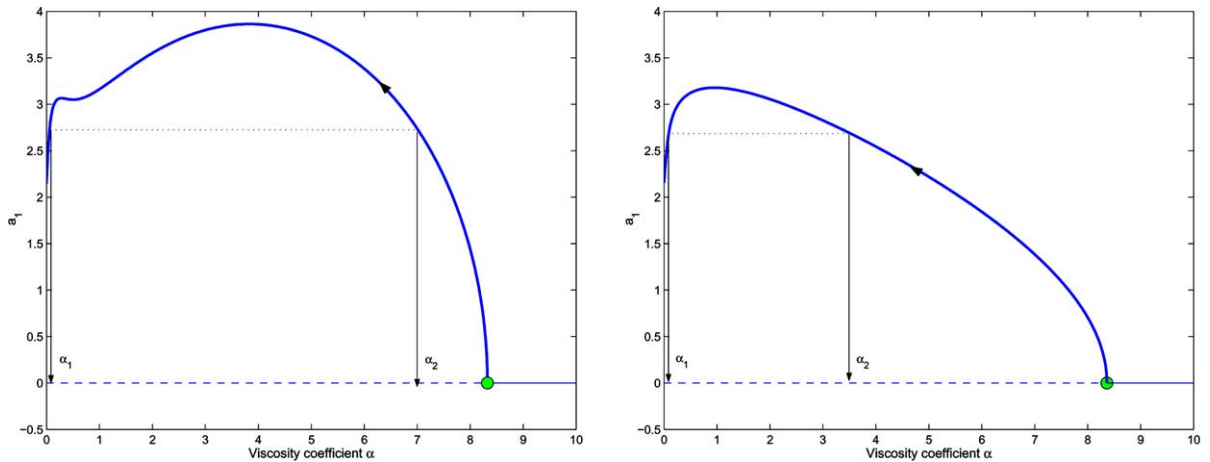


Fig. 13. Bifurcation diagrams for the 6-mode parameterized SV-POD system at $Re = 100$. Left: $M = 2$ and Right: $M = 4$. The circle denotes the Hopf bifurcation point; on its left is the unstable region (dashed line) and on its right is the stable region (thin line).

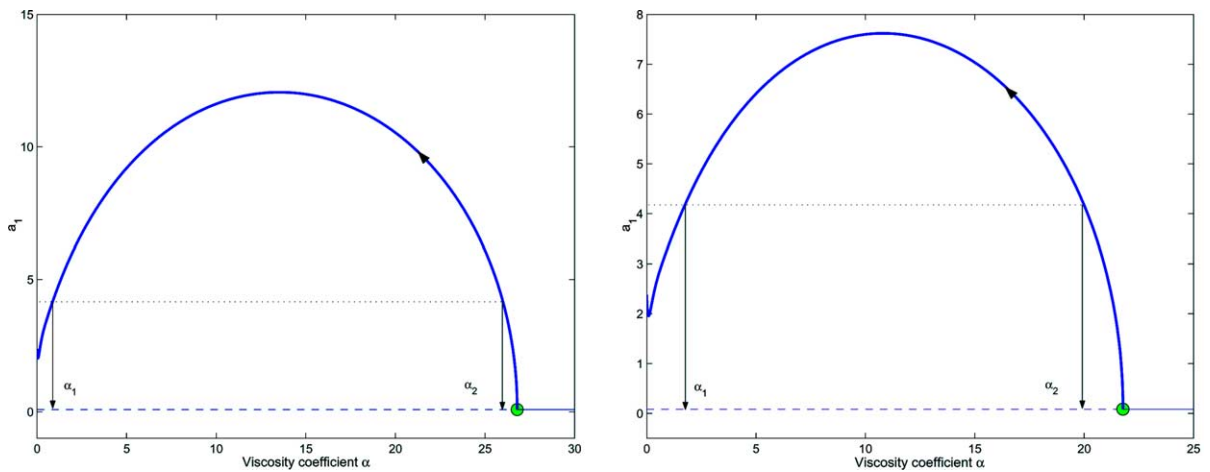


Fig. 14. Bifurcation diagrams for the 6-mode parameterized SV-POD system at $Re = 500$. Left: $M = 2$ and Right: $M = 4$. The circle denotes the Hopf bifurcation point; on its left is the unstable region (dashed line) and on its right is the stable region (thin line).

Once the best value of the viscosity coefficient is obtained, simulations are performed to confirm the results of the bifurcation analysis. In Figs. 15 (upper) and 16 (upper) we plot the results of the POD simulation at $Re = 100$ and 500, respectively, using the parameterized SV model for the 6-mode system. Long-time integration confirms the accuracy of the system consistent with the bifurcation analysis. From these plots we can also see that the $Re = 100$ case is simulated very accurately including the high modes unlike the higher Reynolds number case. For the latter, good agreement is achieved only for the first two modes whereas the higher modes appear overly damped.

We now turn our attention to the case that no Hopf bifurcation point can be found via the bifurcation analysis, as is the case for the *standard* SV-POD system for which only the cut-off $M = 0$ at $Re = 100$ exhibits a bifurcation point. It turns out that in this case too we can select rigorously the viscosity amplitude α . To this end, we can take advantage of the fact that for $\alpha = 0$ we have an asymptotically stable periodic

Table 4

Best viscosity coefficient α at different cut-off modes M for the 6-mode parameterized SV-POD system

Re	Cut-off (M)	Coefficient (α_1)	Period (T_1)	Coefficient (α_2)	Period (T_2)
100	0	4.833E-02	5.877	3.060E-01	5.871
100	2	5.562E-02	5.877	7.096	5.872
100	4	9.644E-02	5.874	3.639	5.870
500	0	N/A	N/A	N/A	N/A
500	2	8.999E-01	4.3466	2.598E+01	4.3451
500	4	1.788	4.3484	1.996E+01	4.3454

solution albeit an erroneous one. However, we can perform the bifurcation analysis forward for $\alpha \geq 0$ starting from the zero point. Figs. 17 and 18 show the corresponding bifurcation diagram for the standard SV model for cut-off $M = 2$ and 4 at the two Reynolds number $Re = 100$ and $Re = 500$, respectively. Here too we use the same criteria for selection as before, namely matching of the first and second modal amplitudes and also of the Strouhal period derived from the DNS results.

A summary of the results of the bifurcation analysis is presented in Table 5. Here “N/A” implies that there is no intersection of the first modal amplitude and the periodic branch and thus a matching asymptotically stable periodic solution cannot be found for $M = 0$ at $Re = 500$. The viscosity coefficients from the bifurcation analysis are then used in the POD simulation to obtain the time periodic solutions. The results, plotted in terms of phase portraits, are shown in Figs. 15 (lower) and 16 (lower). All solutions are stable after long time integration consistent with the values of the associated non-trivial Floquet multipliers, which are listed in Table 6.

5.3. Higher resolution SV-POD systems

Next, we study the previous two cases using higher resolution corresponding to a 10-mode POD system for $Re = 100$ and to a 12-mode POD system for $Re = 500$.

First, we analyze the accuracy of the POD systems without including the SV contribution. In Table 7 we present a summary of the results for both Reynolds numbers. We see that in both cases there exist periodic asymptotic states, which are stable since the magnitudes of all Floquet multipliers (after the first one) are below unity. However, these asymptotic states are different from the correct ones that DNS predicts.

We now study the behavior of the parameterized SV-POD system. A summary of the bifurcation analysis results is presented in Table 8. Typical bifurcation diagrams for the cut-off mode $M = 0$ are shown in Fig. 19. The bifurcation analysis reveals that as we vary the viscosity coefficient the parameterized SV-POD always gives a Hopf bifurcation point, thus allowing us to track the periodic solution branch. However, for $Re = 100$ only at cut-off modes $M = 0$ and $M = 2$ we obtained accurately matching asymptotically stable periodic solutions. For $Re = 500$ the only accurate solution is at $M = 0$.

We now turn our attention to the standard SV-POD model for which no Hopf bifurcation points were found. As before, we track the periodic branch forward from $\alpha = 0$ for which there exist stable periodic states although inaccurate. From the bifurcation analysis, it is found that for the standard SV-POD system a matching asymptotically stable solution can be obtained for cut-off mode $M = 0, 2$ and 4. However, with cut-off mode from $M = 6$ to 8 (and correspondingly $M = 4$ to 10 at $Re = 500$), the standard SV-POD model cannot provide a matching stable periodic solution. These results are summarized in Table 9 and typical bifurcation diagrams for $M = 0$ are presented in Fig. 20. The accuracy of the model improves somewhat but not dramatically. In particular, for the $Re = 500$ the high modes improve only slightly over the results presented in Fig. 16. We will discuss this issue further in the next section.

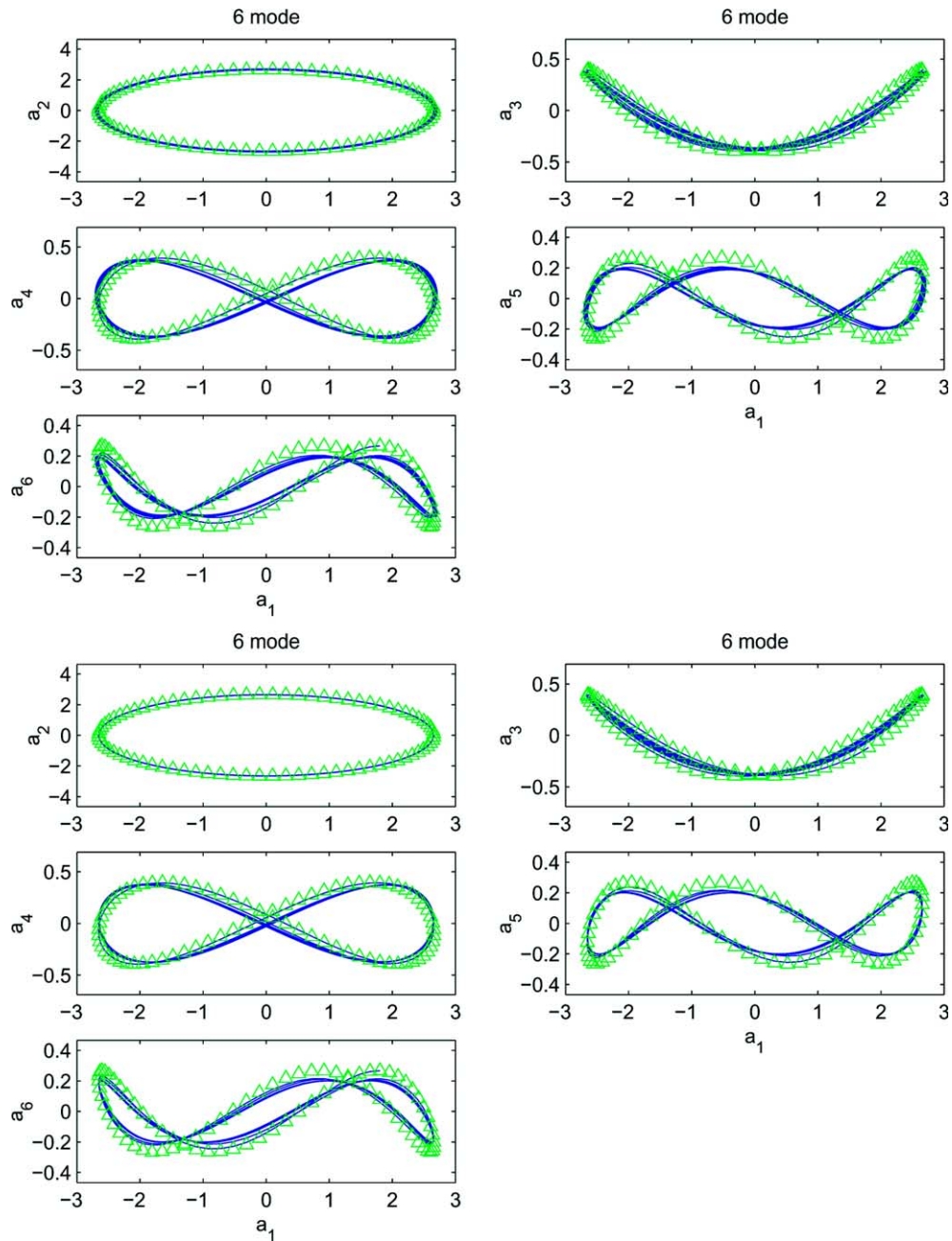


Fig. 15. $Re = 100$. Phase portrait obtained from a simulation based on the 6-mode SV-POD system employing the best value of the viscosity coefficient α and cut-off $M = 2$. Upper: parameterized SV. Lower: standard SV.

We have shown that the long-term prediction of both lower and higher resolution are improved as we use either the parameterized SV or the standard SV with the most effective viscosity coefficient. The question now is if the short-term prediction of these models is affected. In Table 10, we present results that

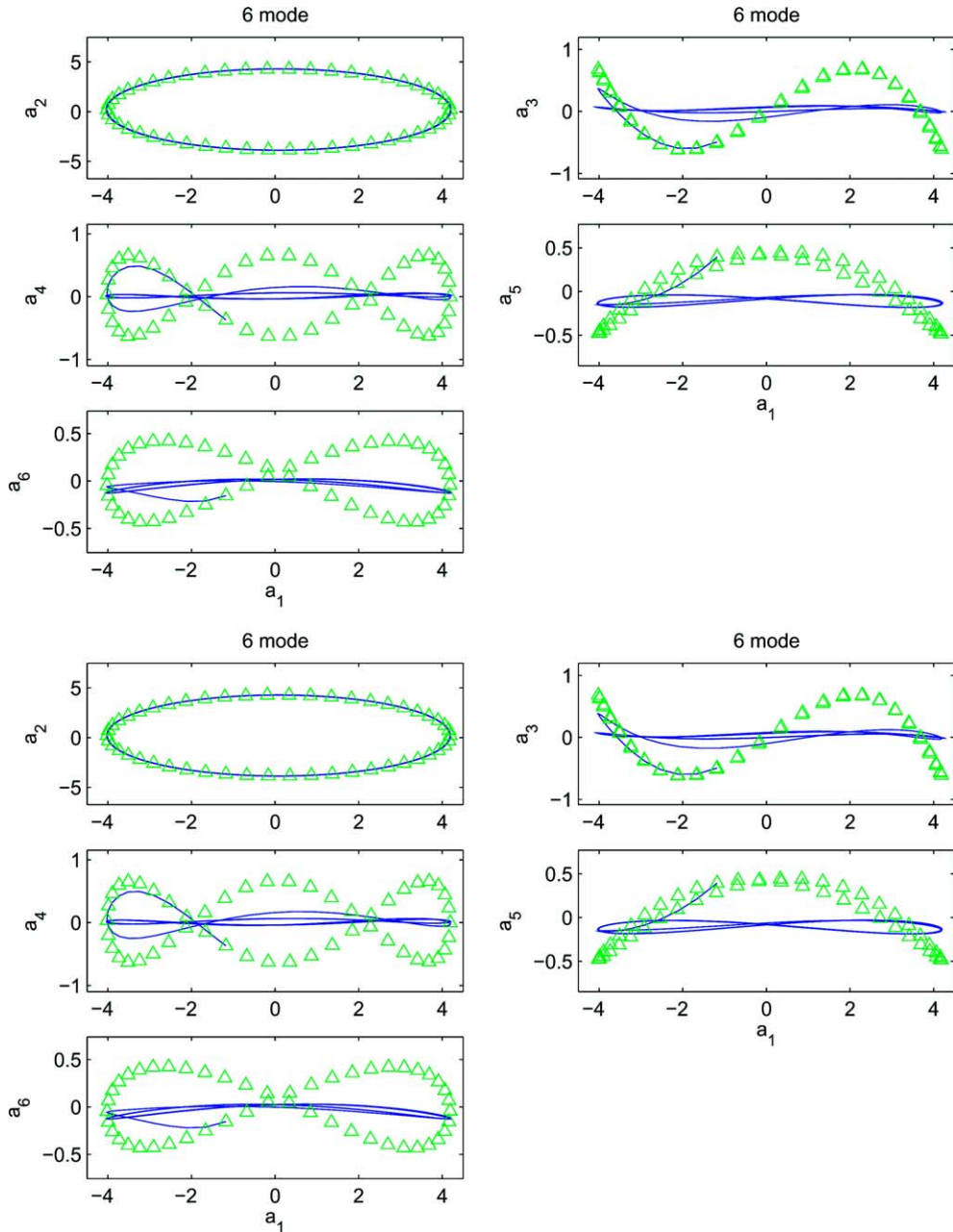


Fig. 16. $Re = 500$. Phase portrait obtained from a simulation based on the 6-mode SV-POD system employing the best value of the viscosity coefficient α and cut-off $M = 2$. Upper: parameterized SV. Lower: standard SV.

show that the accuracy of the prediction of short-term dynamics with the new models is somewhat worse. This comparison assumes that we initialize both types of models with the correct DNS data. If random initial data are selected, the standard POD model will fail to predict either the short-term or the long-term dynamics.

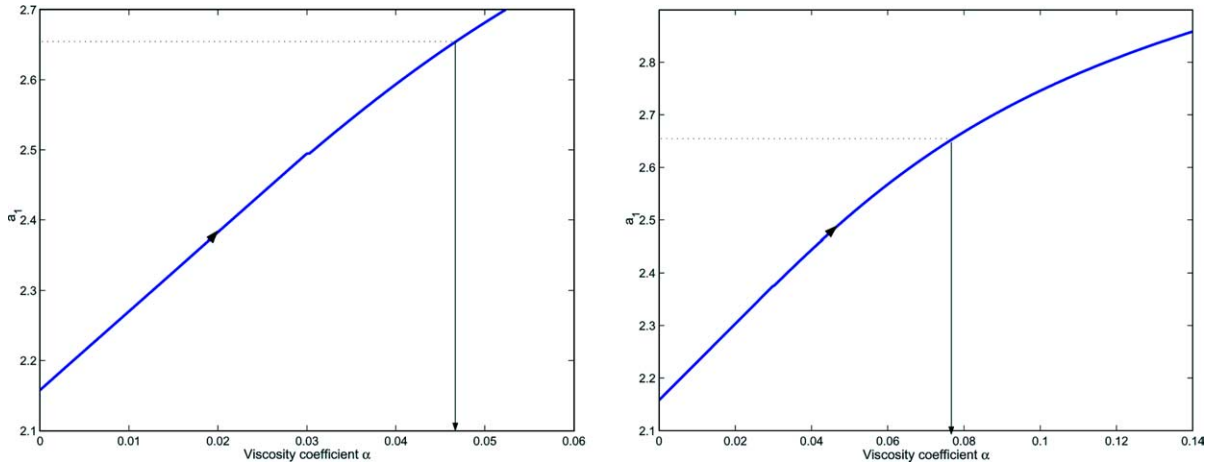


Fig. 17. Bifurcation diagrams for the 6-mode standard SV-POD system at $Re = 100$. Left: $M = 2$ and Right: $M = 4$.

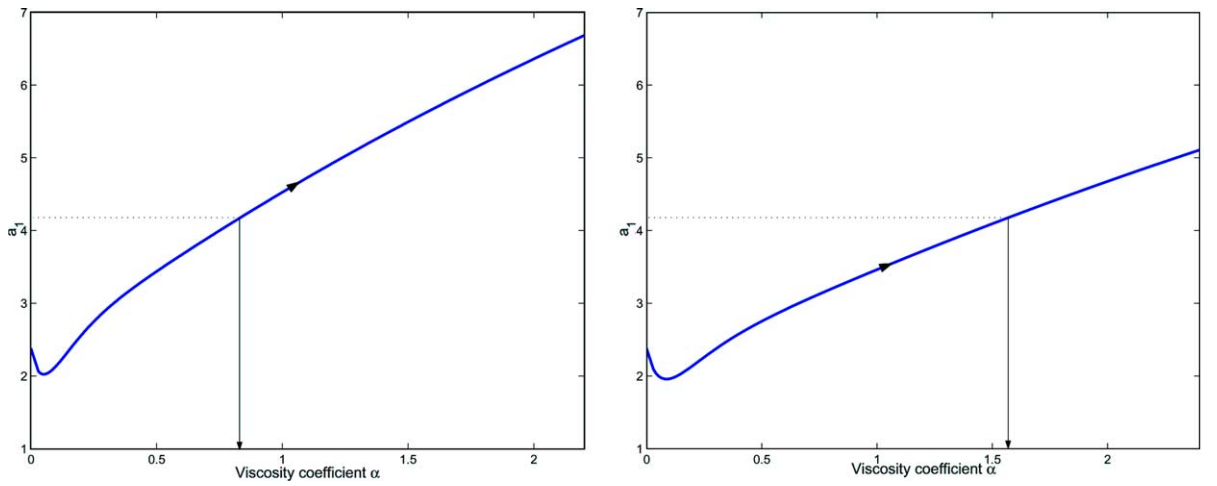


Fig. 18. Bifurcation diagrams for the 6-mode standard SV-POD system at $Re = 500$. Left: $M = 2$ and Right: $M = 4$.

Table 5
Best viscosity coefficient at different cut-off mode M for the 6-mode standard SV-POD model

Re	Cut-off (M)	Coefficient (α)	Period (T)
100	0	2.807E-02	5.877
100	2	4.630E-02	5.878
100	4	7.626E-02	5.876
500	0	N/A	N/A
500	2	8.394E-01	4.346
500	4	1.578	4.3487

Table 6
Floquet multipliers for the solutions presented in Figs. 15 and 16 (lower plots)

$Re = 100$		$Re = 500$	
Parameterized SV	Standard SV	Parameterized SV	Standard SV
9.788E-01	9.790E-01	9.869E-01	9.864E-01
3.621E-01 + 7.606E-02i	3.898E-01 + 7.636E-02i	-5.655E-03 + 1.375E-02i	-6.122E-03 - 1.721E-02i
3.621E-01 - 7.606E-02i	3.898E-01 - 7.636E-02i	-5.655E-03 - 1.375E-02i	-6.122E-03 + 1.721E-02i
-3.266E-01 + 1.485E-02i	-3.544E-01 + 2.402E-02i	-8.973E-09 - 1.215E-08i	-3.144E-08 - 4.321E-08i
-3.266E-01 - 1.485E-02i	-3.544E-01 - 2.402E-02i	-8.973E-09 + 1.215E-08i	-3.144E-08 + 4.321E-08i

Table 7
Asymptotically stable periodic solution of the original POD system for the 10-mode system at $Re = 100$ and the 12-mode system at $Re = 500$

$Re = 100$			$Re = 500$		
Period	Magnitudes	Multipliers	Period	Magnitudes	Multipliers
$T = 5.84$	$\bar{a}_1 = 16.52$ $\bar{a}_2 = 16.67$	7.788E-01	$T = 4.33$	$\bar{a}_1 = 2.29$ $\bar{a}_2 = 2.41$	9.492E-01
		2.023E-01			6.426E-01 - 4.580E-01i
	1.902E-01	6.426E-01 + 4.580E-01i			
	2.931E-01 - 4.818E-01i	-7.560E-01 - 2.142E-01i			
	2.931E-01 + 4.818E-01i	-7.560E-01 + 2.142E-01i			
	-1.112E-01 - 3.189E-01i	-4.918E-01 + 3.165E-01i			
	-1.112E-01 + 3.189E-01i	-4.918E-01 - 3.165E-01i			
	-2.291E-02 - 1.528E-01i	-5.332E-01 + 8.302E-02i			
	-2.291E-02 + 1.528E-01i	-5.332E-01 - 8.302E-02i			
				5.246E-01 + 6.266E-03i	
		5.246E-01 - 6.266E-03i			

Shown are the first two most energetic modal amplitudes and non-trivial Floquet multipliers.

Table 8
Best viscosity coefficient for the high-resolution parameterized SV-POD model

Re	Cut-off (M)	Coefficient (α_1)	Period (T_1)	Coefficient (α_2)	Period (T_2)
100	0	5.377E-02	5.885	3.460	5.866
100	2	3.302E-01	5.877	5.122	5.853
100	4	N/A	N/A	N/A	N/A
100	6	N/A	N/A	N/A	N/A
100	8	N/A	N/A	N/A	N/A
500	0	1.226E+01	4.347	2.974E+01	4.346
500	2	N/A	N/A	N/A	N/A
500	4	N/A	N/A	N/A	N/A
500	6	N/A	N/A	N/A	N/A
500	8	N/A	N/A	N/A	N/A
500	10	N/A	N/A	N/A	N/A

6. Summary and discussion

We have developed a spectral viscosity (SV) method that improves significantly the accuracy of long-term predictions of reduced order models derived from Galerkin projections of evolution equations. Specifically, here we have considered the external flow past a cylinder and investigated the accuracy of the

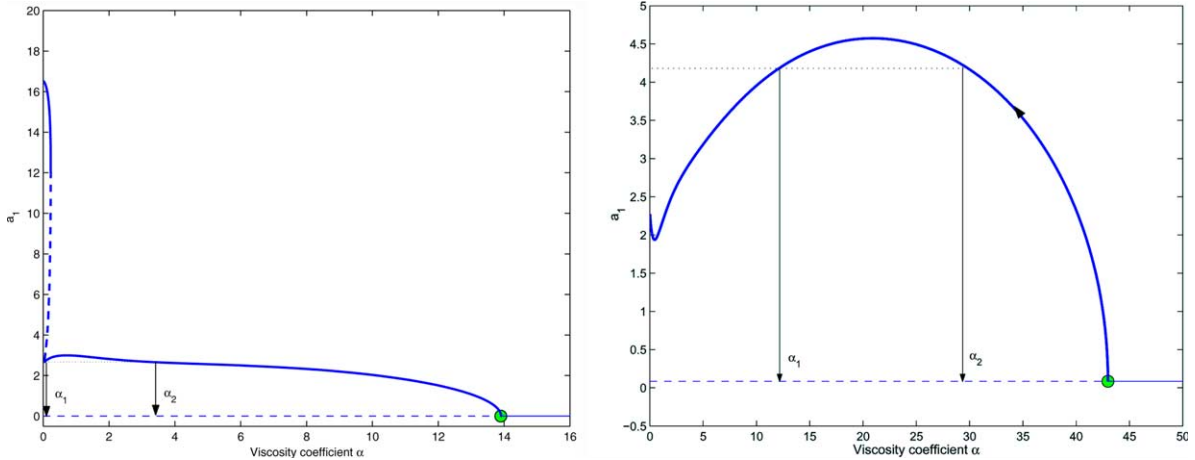


Fig. 19. Bifurcation diagrams for the high-resolution parameterized SV-POD systems at $M = 0$. Left: $Re = 100$. Right: $Re = 500$. The circle denotes the Hopf bifurcation point; on its left is the unstable region (dashed line) and on its right is the stable region (thin line).

Table 9

Best viscosity coefficient for the high-resolution standard SV-POD model

Re	Cut-off (M)	Coefficient (α)	Period (T)
100	0	6.598E - 02	5.885
100	2	2.485E - 01	5.880
100	4	1.029	5.875
100	6	N/A	N/A
100	8	N/A	N/A
500	0	8.195	4.3483
500	2	1.856E + 02	4.349
500	4	N/A	N/A
500	6	N/A	N/A
500	8	N/A	N/A
500	10	N/A	N/A

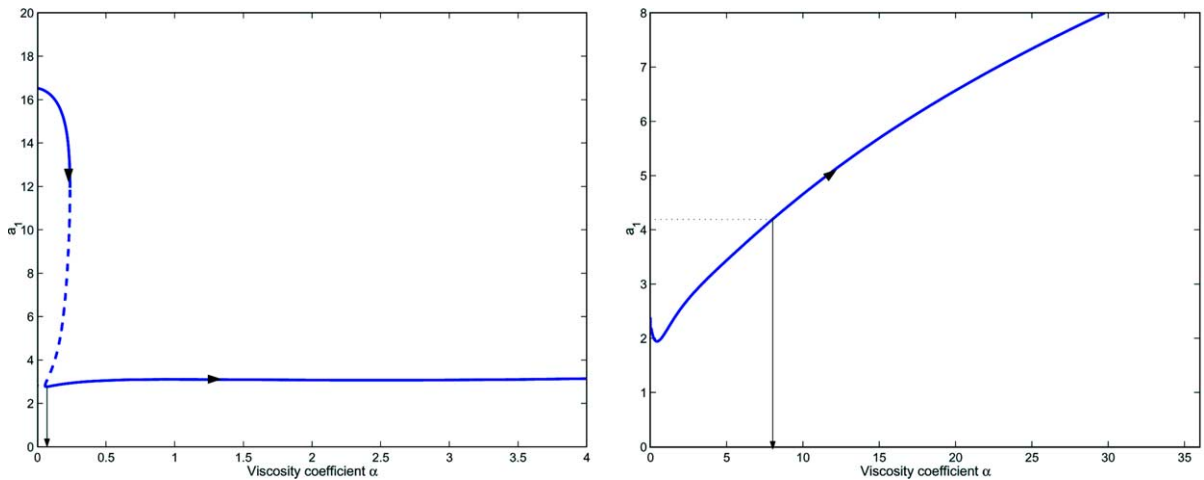


Fig. 20. Bifurcation diagrams for the high-resolution standard SV-POD systems at $M = 0$. Left: $Re = 100$. Right: $Re = 500$.

Table 10

Comparison of the time-averaged error for the first four energetic modes for a short-time simulation of POD, parameterized SV-POD and standard SV-POD ($Re = 100$ and $N = 6$)

L^2 Error	POD ($T = 5.88$)	Standard SV ($T = 5.877$)	Parameterized SV ($T = 5.877$)
\bar{a}_1	0.001673	0.002069	0.002603
\bar{a}_2	0.001869	0.001874	0.002225
\bar{a}_3	0.005664	0.01513	0.01338
\bar{a}_4	0.006879	0.01844	0.01742

limit cycle obtained from a POD-based Galerkin system at two values of Reynolds number. We have found that after very long time integration, all Galerkin models we tested converged to erroneous states, even though they were initialized with the correct state. However, in previous similar studies, where short to modest length time integration was involved, it was shown that such models predict the correct dynamics but it was incorrectly assumed that are asymptotically accurate. The present simulations show that even though the correct dynamics may be predicted for hundreds of shedding cycles (initializing with the correct conditions) eventually a divergence arises. It does not manifest itself as an explosive growth that leads to blow-up but rather as a drift leading to another spurious limit cycle. The precise onset of this divergence depends on the number of modes retained in the model and the Reynolds number as well as the flow geometry.

To this end, we have introduced a modification to the spectral vanishing viscosity (SVV), which has been shown to be effective in preserving monotonicity in hyperbolic conservation laws [20]. SVV is represented by a convolution viscosity kernel, which is parameterized by a viscosity amplitude $\epsilon = \alpha/N$ (where N is the number of retained modes) and a cut-off mode $M < N$. The proper choice of these parameters would guarantee stability without influencing the convergence rate of the POD expansion adversely. However, their exact values are not known *a priori* and they depend on the flow geometry as well as the retained number of POD modes N . In the original SVV the viscosity amplitude is vanishing as the number of modes increases, however in this work we find that this is inappropriate for severely truncated systems.

The new contribution of this work is the use of bifurcation analysis to choose the SV parameters in order to guarantee asymptotic stability. Specifically, the stability of SV-POD systems has been analyzed with respect to the viscosity coefficient α as bifurcation parameter. Parametric studies with respect to the cut-off mode M yield the most effective pair (α, M) that fully characterizes the SV model. In particular, we constructed bifurcation diagrams for the standard SV model starting from the point $\epsilon = \alpha = 0$, which belongs to a periodic branch, and searching forward for $\alpha > 0$. This procedure produces a stable periodic branch for each of the SV-POD models tested. An alternative method we developed is to perturb slightly the SV model to exhibit a Hopf bifurcation point unlike the standard SV model that does not exhibit such points. Subsequently, we follow that bifurcation point to track the periodic branch with respect to α as before.

There are infinitely many candidate states on the stable periodic branch, and selection of the proper state is a matter of careful modeling of the flow system that we study. For the flow past a cylinder that we consider here, its POD eigenspectrum decays very fast (see Fig. 3) and thus the first couple of modes dominate the dynamics. To this end, we have used the amplitude of the first mode to intersect its periodic branch in the corresponding bifurcation diagram, thus obtaining a definitive value of the viscosity amplitude in the SV model. Due to the approximately traveling-wave form of the vortex street, the eigenvalues form pairs and thus the second eigenmode matches as well. For fast decaying eigenspectra the rest of the eigenmodes agree with the DNS results, although the higher ones (modes greater than the cut-off mode M) are affected adversely. Clearly, this decision for selecting the amplitude does not guarantee that ϵ will vanish monotonically with the number of modes N , as in the original SVV method.

For flat spectra the procedure we adopted here may not be the optimum one. This was evident to some degree for the $Re = 500$ case we studied in the current work, where the high modes were not in good

agreement with the DNS results. An alternative procedure in improving accuracy in this case could be formulated by following a least-squares approach or minimizing an appropriate objective function. One possibility is to use the weighted sum of the squared differences in the modal amplitudes, where the weights could be the normalized POD eigenvalues. Other flow systems may require different treatment. The point we want to emphasize, however, is that after establishing a limit cycle with the SV-POD model, additional criteria need to be employed to improve the accuracy of the prediction.

The SVV non-linear stability theory is based on the treatment of the inviscid Burgers equation, originally proposed by Tadmor [20] for Fourier discretization. We can justify its use in the current context only heuristically and have been motivated by success in other applications [21,23]. However, a rigorous justification for low-dimensional models derived from Galerkin projections is currently missing, and thus we do not have much insight into the effectiveness of SVV. The extra term appearing in Eq. (7), in addition to the standard viscosity term, is perhaps the key but its optimum form may depend on the specific dissipative PDE considered. For example, by perturbing the original SVV model of Tadmor in the current work we produced a new dynamic response, with the modified system exhibiting Hopf bifurcation points unlike the original one. Future work should address these issues, and also investigate the dissipation spectrum in detail for larger systems with higher number of modes so that a sufficient dissipation range exists. Finally, correcting the long-term behavior of the POD model does not imply that the model can correctly capture the correct bifurcation dynamics of the flow. To this end, a hybrid basis consisting of snapshots taken at both sides of the bifurcation point should be employed, see [27].

Acknowledgements

The first author gratefully acknowledges the DPST (Development and Promotion of Science and Technology Talents) project from Thailand for providing his scholarship during his graduate studies at Brown University. This work was supported by ONR and NSF, and computations were performed at the facilities of NCSA (University of Illinois at Urbana-Champaign) and at DoD's NAVO MSRC. The authors would like to acknowledge helpful discussions with Dr. Xia Ma.

References

- [1] G. Bekooz, P. Holmes, J.L. Lumley, The proper orthogonal decomposition in the analysis of turbulent flows, *Ann. Rev. Fluid Mech.* 25 (1993) 539–575.
- [2] L. Sirovich, Turbulence and the dynamics of coherent structures, Parts I, II and III, *Quart. Appl. Math.* XLV (1987) 561–590.
- [3] A. Glezer, Z. Kadioglu, A.J. Pearlstein, Development of an extended proper orthogonal decomposition and its application to a time periodically forced plane mixing layer, *Phys. Fluids* 1 (8) (1989) 1363.
- [4] J.H. Citriniti, W.K. George, Reconstruction of the global velocity field in the axisymmetric mixing layer utilizing the proper orthogonal decomposition, *J. Fluid Mech.* 418 (2000) 137–166.
- [5] R.E. Arndt, D.F. Long, M.N. Glauser, The proper orthogonal decomposition of pressure fluctuations surrounding a turbulent jet, *J. Fluid Mech.* 340 (1997) 1–33.
- [6] S.V. Gordeyev, F.O. Thomas, Coherent structure in the turbulent planar jet. Part 1. Extraction of proper orthogonal decomposition eigenmodes and their self-similarity, *J. Fluid Mech.* 414 (2000) 145–194.
- [7] J. Delville, L. Ukeiley, L. Cordier, J.P. Bonnet, M. Glauser, Examination of large-scale structures in a turbulent plane mixing layer. Part 1. Proper orthogonal decomposition, *J. Fluid Mech.* 391 (1999) 91–122.
- [8] A.E. Deane, I.G. Kevrekidis, G.E. Karniadakis, S.A. Orszag, Low-dimensional models for complex geometry flows: application to grooved channels and circular cylinders, *Phys. Fluids A* 3 (10) (1991) 2337–2354.
- [9] N. Aubry, P. Holmes, J.L. Stone, J.L. Lumley, The dynamics of coherent structures in the wall region of a turbulent boundary layer, *J. Fluid Mech.* 192 (1988) 115–173.
- [10] D. Rempfer, H.F. Fasel, Evolution of three-dimensional coherent structures in a flat-plate boundary layer, *J. Fluid Mech.* 260 (1994) 351–375.

- [11] A. Liakopoulos, P.A. Blythe, H. Gunes, A reduced dynamical model of convective flows in tall laterally heated cavities, *Proc. R. Soc. Lond. A* 453 (1997) 663–672.
- [12] W. Cazemier, R.W. Verstappen, A.E. Veldman, Proper orthogonal decomposition and low-dimensional models for driven cavity flows, *Phys. Fluids* 10 (7) (1998) 1685–1699.
- [13] S.N. Singh, H.M. James, A.A. Gregory, B. Siva, K.H. James, Optimal feedback control of vortex shedding using proper orthogonal decomposition models, *Trans. ACME* 123 (2001) 612–618.
- [14] C. Foias, M.S. Jolly, I.G. Kevrekidis, E.S. Titi, Dissipativity of the numerical schemes, *Nonlinearity* 4 (1991) 591–613.
- [15] M.S. Jolly, I.G. Kevrekidis, E.S. Titi, Preserving dissipation in approximate inertial manifolds for the Kuramoto–Sivashinsky equation: analysis and computations, *J. Dynam. Diff. Eq.* 3 (1991) 179–197.
- [16] M. Marion, R. Temam, Nonlinear Galerkin methods, *SIAM J. Numer. Anal.* 26 (1989) 1139–1157.
- [17] A. Debussche, T. Dubois, R. Temam, The nonlinear Galerkin method: a multiscale method applied to the simulation of homogeneous turbulent flows, *Theor. Comp. Fluid. Dyn.* 7 (1995) 279–299.
- [18] J. Shen, Long time stability and convergence for fully discrete nonlinear Galerkin methods, *Appl. Anal.* 38 (1989) 201–229.
- [19] X. Ma, G.E. Karniadakis, H. Park, M. Gharib, DPIV-driven simulation: a new computational paradigm, *Proc. R. Soc. Lond. A* 459 (2003) 547–565.
- [20] E. Tadmor, Convergence of spectral methods for nonlinear conservation laws, *SIAM J. Numer. Anal.* 26 (1) (1989) 30–44.
- [21] G.S. Karamanos, G.E. Karniadakis, A spectral vanishing viscosity method for large-eddy simulations, *J. Comp. Phys.* 162 (2000) 22–50.
- [22] S.M.O. Kaber, A Legendre pseudospectral viscosity method, *J. Comput. Phys.* 128 (1996) 165–180.
- [23] O. Andreassen, I. Lie, C.E. Wasberg, The spectral viscosity method applied to simulation of waves in a stratified atmosphere, *J. Comput. Phys.* 110 (1994) 257–273.
- [24] E. Tadmor, Super viscosity and spectral approximations of nonlinear conservation laws, in: M.J. Baines, K.W. Morton (Eds.), *Numerical Methods for Fluid Dynamics, IV*, Clarendon Press, Oxford, 1993, p. 69.
- [25] H.-P. Ma, Chebyshev–Legendre spectral viscosity method for nonlinear conservation laws, *SIAM J. Numer. Anal.* 35 (3) (1998) 869–892.
- [26] H.-P. Ma, Chebyshev–Legendre super spectral viscosity method for nonlinear conservation laws, *SIAM J. Numer. Anal.* 35 (3) (1998) 893–908.
- [27] X. Ma, G.E. Karniadakis, A low-dimensional model for simulating 3d cylinder flow, *J. Fluid Mech.* 458 (2002) 181–190.
- [28] G.E. Karniadakis, S.J. Sherwin, *Spectral/hp Element Methods for CFD*, Oxford University Press, 1999.
- [29] N. Aubry, W.Y. Lian, E.S. Titi, Preserving symmetries in the proper orthogonal decomposition, *SIAM J. Sci. Comput.* 14 (2) (1993) 483–505.
- [30] S. Sirisup, Convergence and stability of low-dimensional flow models, Ph. D. Thesis, Division of Applied Mathematics, Brown University, in progress.
- [31] M.G. Crandall, P.L. Lions, Viscosity solutions of Hamilton–Jacobi equations, *Trans. Am. Math. Soc.* 277 (1983) 1–42.
- [32] Y. Maday, S.M. Ould Kaber, E. Tadmor, Legendre pseudospectral viscosity method for nonlinear conservation laws, *SIAM J. Numer. Anal.* 30 (1993) 321–342.
- [33] E. Tadmor, Total variation and error estimates for spectral viscosity approximations, *Math. Comp.* 60 (1993) 245.
- [34] E.J. Doedel, R.C. Paffenroth, A.R. Champneys, T.F. Fairgrieve, Yu.A. Kuznetsov, B. Sandstede, X. Wang, *Auto 2000: Continuation and bifurcation software for ordinary differential equations (with homcont)*, Technical Report, Caltech, 2001.